

See discussions, stats, and author profiles for this publication at: <https://www.researchgate.net/publication/272075242>

# Proton Conduction and Long-Range Ferrimagnetic Ordering in Two Isostructural Copper(II) Mesoxalate Metal–Organic Frameworks

ARTICLE in INORGANIC CHEMISTRY · FEBRUARY 2015

Impact Factor: 4.76 · DOI: 10.1021/ic502586a · Source: PubMed

---

CITATIONS

3

READS

87

## 6 AUTHORS, INCLUDING:



Beatriz Gil-Hernández

Universidad de La Laguna

13 PUBLICATIONS 272 CITATIONS

[SEE PROFILE](#)



Pedro Núñez

Universidad de La Laguna

213 PUBLICATIONS 3,172 CITATIONS

[SEE PROFILE](#)



Christoph Janiak

Heinrich-Heine-Universität Düsseldorf

385 PUBLICATIONS 13,834 CITATIONS

[SEE PROFILE](#)



Joaquín Sanchiz

Universidad de La Laguna

84 PUBLICATIONS 2,661 CITATIONS

[SEE PROFILE](#)

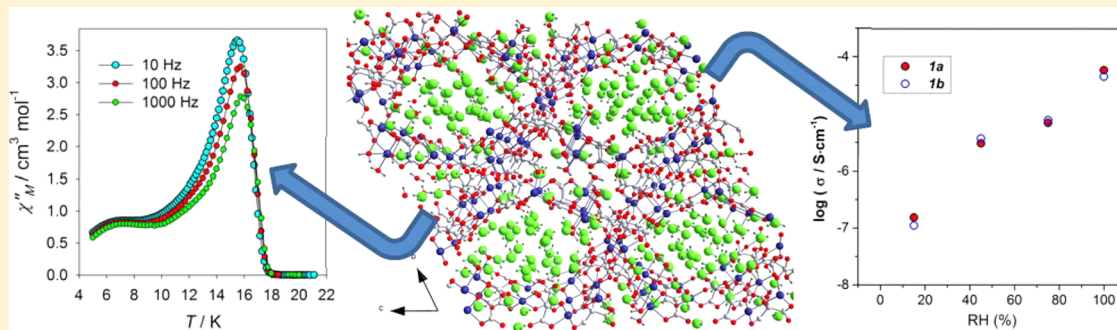
# Proton Conduction and Long-Range Ferrimagnetic Ordering in Two Isostructural Copper(II) Mesoxalate Metal–Organic Frameworks

Beatriz Gil-Hernández,<sup>†</sup> Stanislav Savvin,<sup>†</sup> Gamall Makhloifi,<sup>‡</sup> Pedro Núñez,<sup>†</sup> Christoph Janiak,<sup>‡</sup> and Joaquín Sanchiz<sup>\*†</sup>

<sup>†</sup>Departamento de Química, Facultad de Ciencias, Universidad de La Laguna, 38206 La Laguna, Tenerife, Spain

<sup>‡</sup>Universität Düsseldorf, Institut für Anorganische Chemie und Strukturchemie, Universitätsstr. 1, D-40225 Düsseldorf, Germany

## Supporting Information



**ABSTRACT:** Two compounds of formula  $\{(\text{H}_3\text{O})[\text{Cu}_7(\text{Hmesox})_5(\text{H}_2\text{O})_7]\cdot 9\text{H}_2\text{O}\}_n$  (**1a**) and  $\{(\text{NH}_4)_{0.6}(\text{H}_3\text{O})_{0.4}[\text{Cu}_7(\text{Hmesox})_5(\text{H}_2\text{O})_7]\cdot 11\text{H}_2\text{O}\}_n$  (**1b**) were prepared and structurally characterized by single-crystal X-ray diffraction ( $\text{H}_4\text{mesox}$  = mesoxalic acid, 2-dihydroxymalonic acid). The compounds are crystalline functional metal–organic frameworks exhibiting proton conduction and magnetic ordering. Variable-temperature magnetic susceptibility measurements reveal that the copper(II) ions are strongly ferro- and antiferromagnetically coupled by the alkoxide and carboxylate bridges of the mesoxalate linker to yield long-range magnetic ordering with a  $T_c$  of 17.6 K, which is reached by a rare mechanism known as topologic ferrimagnetism. Electric conductivity, measured by impedance methods, shows values as high as  $6.5 \times 10^{-5} \text{ S cm}^{-1}$  and occurs by proton exchange among the hydronium/ammonium and water molecules of crystallization, which fill the voids left by the three-dimensional copper(II) mesoxalate anionic network.

## INTRODUCTION

Metal–organic frameworks (MOFs) are crystalline, potentially porous materials in which metal ions, or metal clusters, are linked by organic ligands to yield infinite metal–ligand networks.<sup>1–5</sup> Lately, much attention has been paid to this class of materials because of their interesting properties such as nonlinear optics, luminescence, chirality, drug delivery, sensor technology as well as surface properties like gas storage, separation, and catalysis.<sup>6–20</sup> Moreover, organic ligands with linkers constituted by a low number of atoms such as oxalate,<sup>21–24</sup> oxamate,<sup>25,26</sup> or cyanide<sup>27–30</sup> offer an electronic pathway for magnetic superexchange interactions, and MOFs constructed with these linkers and paramagnetic ions may exhibit interesting magnetic properties.

More recently, studies of the inherent porosity of these materials began for the development of proton-conducting membranes for fuel cells and also for the better understanding of the proton transport dynamics.<sup>31–46</sup> Proton conduction in MOFs has been found to reach values up to  $4.2 \times 10^{-2} \text{ S cm}^{-1}$ ,<sup>47,48</sup> a value very close to that achieved by ceramic proton conductors, which operate at much higher temperatures (600–1000 °C).<sup>49</sup>

Nowadays, one of the challenges for researchers in this field consists of the combination of some of the above properties together to yield functional materials. Among them, those merging proton-conduction and long-range magnetic ordering have potential technological applications in the field of molecular electronics and spintronics and constitute an emerging field of research.<sup>32,33,43,50–54</sup> These materials require paramagnetic ions connected efficiently by organic linkers and to end up in an open metal–organic framework whose pores are filled by  $\text{H}^+$  ions, hydrogen acceptors, and crystallization water molecules.<sup>36,55–58</sup> In this sense, carboxylate-bridged functional materials with conductivities up to  $1.1 \times 10^{-3} \text{ S cm}^{-1}$  have been obtained, but with magnetic ordering temperatures of 3.0 K (Table 1).<sup>43</sup> Others with much higher magnetic ordering temperatures,  $T_c = 42–44$  K, exhibit, on the other hand, very low conductivities of  $\sim 10^{-6} \text{ S cm}^{-1}$ .<sup>53</sup> And others, with ordering temperatures up to 12.5 K, show conductivities of  $\sim 8.0 \times 10^{-5} \text{ S cm}^{-1}$ .<sup>32,33,54</sup> So, it appears

Received: October 28, 2014

Published: February 4, 2015

**Table 1. Highest Proton Conductivity ( $\sigma_H$ ) at a Given Temperature (T) and Magnetic Ordering Temperature ( $T_c$ ) of Some Representative Magnetic MOFs**

compound <sup>a</sup>	$\sigma_H$ (S cm <sup>-1</sup> )	T (K)	$T_c$ (K)	reference
(NH(prol) <sub>3</sub> ) <sub>3</sub> [Mn <sup>II</sup> Cr <sup>III</sup> (ox) <sub>3</sub> ]	$\sim 1 \times 10^{-4}$	298	5.5	32
(NH(prol) <sub>3</sub> ) <sub>3</sub> [Fe <sup>II</sup> Cr <sup>III</sup> (ox) <sub>3</sub> ]	$\sim 1 \times 10^{-4}$	298	9.0	32
(NH(prol) <sub>3</sub> ) <sub>3</sub> [Co <sup>II</sup> Cr <sup>III</sup> (ox) <sub>3</sub> ]	$\sim 1 \times 10^{-4}$	298	10.0	32
(NH <sub>4</sub> ) <sub>4</sub> [MnCr <sub>2</sub> (ox) <sub>6</sub> ]	$1.1 \times 10^{-3}$	295	3.0	43
(NEt <sub>3</sub> (CH <sub>2</sub> COOH)) [MnCr(ox) <sub>3</sub> ]	$\sim 1 \times 10^{-4}$	298	5.6	33, 53
(NBu <sub>3</sub> (CH <sub>2</sub> COOH)) [MnCr(ox) <sub>3</sub> ]	$\sim 1 \times 10^{-7}$	298	5.9	33
(NMe <sub>3</sub> (CH <sub>2</sub> COOH)) [FeCr(ox) <sub>3</sub> ]	$\sim 1 \times 10^{-4}$	298	11.0	33
(NBu <sub>3</sub> (CH <sub>2</sub> COOH)) [FeCr(ox) <sub>3</sub> ]	$\sim 1 \times 10^{-5}$	298	12.5	33
(NEt <sub>3</sub> (CH <sub>2</sub> COOH)) [FeFe(ox) <sub>3</sub> ]	$\sim 1 \times 10^{-6}$	298	42	53
(NBu <sub>3</sub> (CH <sub>2</sub> COOH)) [FeFe(ox) <sub>3</sub> ]	$\sim 1 \times 10^{-6}$	298	42	53

<sup>a</sup>NH(prol)<sub>3</sub> = tri(3-hydroxypropyl)ammonium, ox = oxalate, Et = ethyl, Bu = n-butyl

very attractive to prepare these kinds of functional MOFs and to try to maximize their performance.

Previous studies done in our research group showed the mesoxalate ligand (the conjugate base of dihydroxymalonic acid = H<sub>4</sub>mesox) to fit the requirements to yield compounds exhibiting both properties. For instance, the porous heterometallic mesoxalate MOFs {(Ph<sub>4</sub>P)<sub>2</sub>[M<sup>II</sup>Cu<sub>3</sub>(Hmesox)<sub>3</sub>Cl] $\cdot$ xH<sub>2</sub>O}<sub>n</sub> (with M(II) = Mn, Co, and Ni) crystallize in chiral anionic cubic networks with tetraphenylphosphonium cations and crystallization water filling the pores and show magnetic ordering temperatures in the range from 7 to 21 K.<sup>59–61</sup> In addition, the mesoxalate ligand is a good candidate to exhibit proton conduction since it contains carboxylate and alcohol groups that stabilize crystallization water molecules, and the anionic network could be charge-balanced by hydronium cations located in the pores.<sup>45,53,54</sup> Thus, in this work we explore the possibilities of the mesoxalate linker in the preparation of functional materials exhibiting proton conduction and long-range magnetic ordering. We show herein the magnetic and electrical properties of two isostructural compounds with formula {(H<sub>3</sub>O)[Cu<sub>7</sub>(Hmesox)<sub>5</sub>(H<sub>2</sub>O)<sub>7</sub>] $\cdot$ 9H<sub>2</sub>O}<sub>n</sub> (**1a**) and {(NH<sub>4</sub>)<sub>0.6</sub>(H<sub>3</sub>O)<sub>0.4</sub>[Cu<sub>7</sub>(Hmesox)<sub>5</sub>(H<sub>2</sub>O)<sub>7</sub>] $\cdot$ 11H<sub>2</sub>O}<sub>n</sub> (**1b**).

## EXPERIMENTAL SECTION

**Materials and Methods.** All reagents were purchased from commercial sources and used as received. Elemental analyses (CHN) were carried out on a FLASH EA 1112 CHNS-O microanalytical analyzer. IR spectra (KBr disks, 400–4000 cm<sup>-1</sup>) were recorded on a Thermo Nicolet Avatar 360 FT-IR spectrometer. X-ray powder diffraction patterns on polycrystalline samples were collected with a PANalytical X'pert X-ray diffractometer (Cu K $\alpha$  radiation = 1.5418 Å) at room temperature. Thermal analysis was carried out on a PerkinElmer system (model Pyris Diamond TG/DTA) under dinitrogen or air atmosphere with a flow rate of 80 cm<sup>3</sup> min<sup>-1</sup>.

{(H<sub>3</sub>O)[Cu<sub>7</sub>(Hmesox)<sub>5</sub>(H<sub>2</sub>O)<sub>7</sub>] $\cdot$ 9H<sub>2</sub>O}<sub>n</sub> (**1a**). A cation exchange resin (Amberlite IR-120, 3.5 g) was added to a suspension of mesoxalate disodium salt (360 mg, 2 mmol) in 14 mL of water, filtered through a Buchner funnel (porosity 25–50  $\mu$ m) into a round-bottom flask, and allowed to react under stirring with basic copper(II) carbonate (220 mg, 2 mmol) for 20 min at 30 °C. The resultant blue solution was diluted with 4 mL of water, filtered to remove traces of

copper(II) oxide, and followed by the addition of copper(II) nitrate (160 mg, 2/3 mmol). Finally, pH was adjusted to 2.9 by the addition of an aqueous solution of tetrabutylammonium hydroxide (1 M). After a week, prismatic blue single crystals of **1a** were obtained by slow evaporation at 21 °C. Yield 48%. Anal. Calcd for **1a** C<sub>15</sub>H<sub>41</sub>Cu<sub>7</sub>O<sub>47.15</sub> (1417.85): C, 12.69; H, 2.89. Found: C, 12.58; H, 2.84%. IR spectrum main peaks [cm<sup>-1</sup>] 1650–1550 (s, b), 1390 (s), 1391(s), and 1124 (s).

{(NH<sub>4</sub>)<sub>0.6</sub>(H<sub>3</sub>O)<sub>0.4</sub>[Cu<sub>7</sub>(Hmesox)<sub>5</sub>(H<sub>2</sub>O)<sub>7</sub>] $\cdot$ 11H<sub>2</sub>O}<sub>n</sub> (**1b**). As in **1a**, but aqueous ammonia (2 M) was used in place of tetrabutylammonium hydroxide. Yield 55%. Anal. Calcd for C<sub>15</sub>H<sub>44.4</sub>N<sub>0.6</sub>Cu<sub>7</sub>O<sub>48.4</sub> (1452.05): C, 12.40; H, 2.97; N, 0.58; Found: C, 12.50; H, 2.93; N, 0.56%. IR of **1b** is equivalent to that of **1a**.

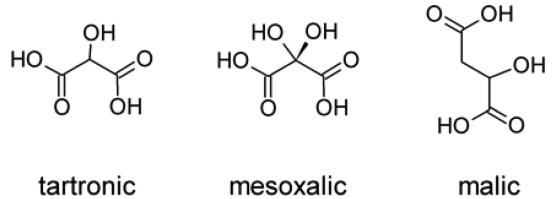
**Magnetic Measurements.** Variable-temperature magnetic susceptibility measurements were carried out on a Quantum Design SQUID MPMS XL magnetometer on polycrystalline samples contained in a calibrated gelatin capsule held at the center of a drinking straw that was fixed at the end of the sample rod. The two parts of the gelatin capsule were mounted in such a way that torquing of crystallites was avoided. Diamagnetic corrections of the constituent atoms were estimated from Pascal's constants,<sup>62</sup> and experimental susceptibilities were also corrected for the temperature-independent paramagnetism and the magnetization of the sample holder. The direct current (dc) measurements were performed in the temperature range of 1.9–300 K at applied magnetic fields of 50, 100, and 500 Oe. The alternating current (ac) measurements were performed at various frequencies (10, 100, and 1000 Hz) with an oscillating field of 3 Oe and a static field of 0 Oe. The Magnetization and the hysteresis loop from -5 to 5 T was measured at 2.00 K.

**Conductometric Measurements.** Electrical conductivity of **1a** and **1b** was studied by impedance spectroscopy. Prior to making measurements, ~0.15 g of the (polycrystalline) sample was pressed at 250 MPa for 2 min. Both faces of the pellets thus obtained were covered with conductive Ag paint (RS Components, USA) and allowed to dry at room temperature for at least 1 h to ensure good adhesion and conductivity. Afterward, each pellet was placed in a gastight sample stage outfitted with an outer quartz housing, gas inlet and outlet tubes, and a thermocouple located in the close vicinity of the sample. The impedance spectra were recorded on a Solartron 1260 impedance/gain-phase analyzer in the frequency range from 1 Hz to 1 MHz. During each measurement root-mean-square ac voltage amplitude was set to 200 mV. The relative humidity of the air fed into the sample stage was controlled by first passing it through a saturated at 23 °C salt solution or deionized water held at the same temperature. Pure water and the saturated solutions of NaCl, K<sub>2</sub>CO<sub>3</sub>, and LiCl ensured 100%, 75%, 45%, and 15% relative humidity, respectively. In some instances the air was passed over freshly dehydrated silica gel before entering the gas inlet. Depending on the relative humidity of the air it took 20 to 250 h for the samples to reach equilibrium conductivity values.

**X-ray Crystallography.** Single-crystal X-ray diffraction (XRD) data were collected at 100(2) K with a Bruker Kappa APEX-II CCD area detector with microfocus sealed tube, Mo K $\alpha$  radiation ( $\lambda$  = 0.71073 Å), and multilayer mirror monochromator for compound **1a** and at 100(2) K with an Agilent SuperNova diffractometer with microfocus X-ray on Cu K $\alpha$  radiation ( $\lambda$  = 1.5418 Å) for **1b**. Crystallographic data collection and refinement parameters are given in Supporting Information, Table S1, with additional details available in CIF format. Crystallographic details are available in CIF format.

## RESULT AND DISCUSSION

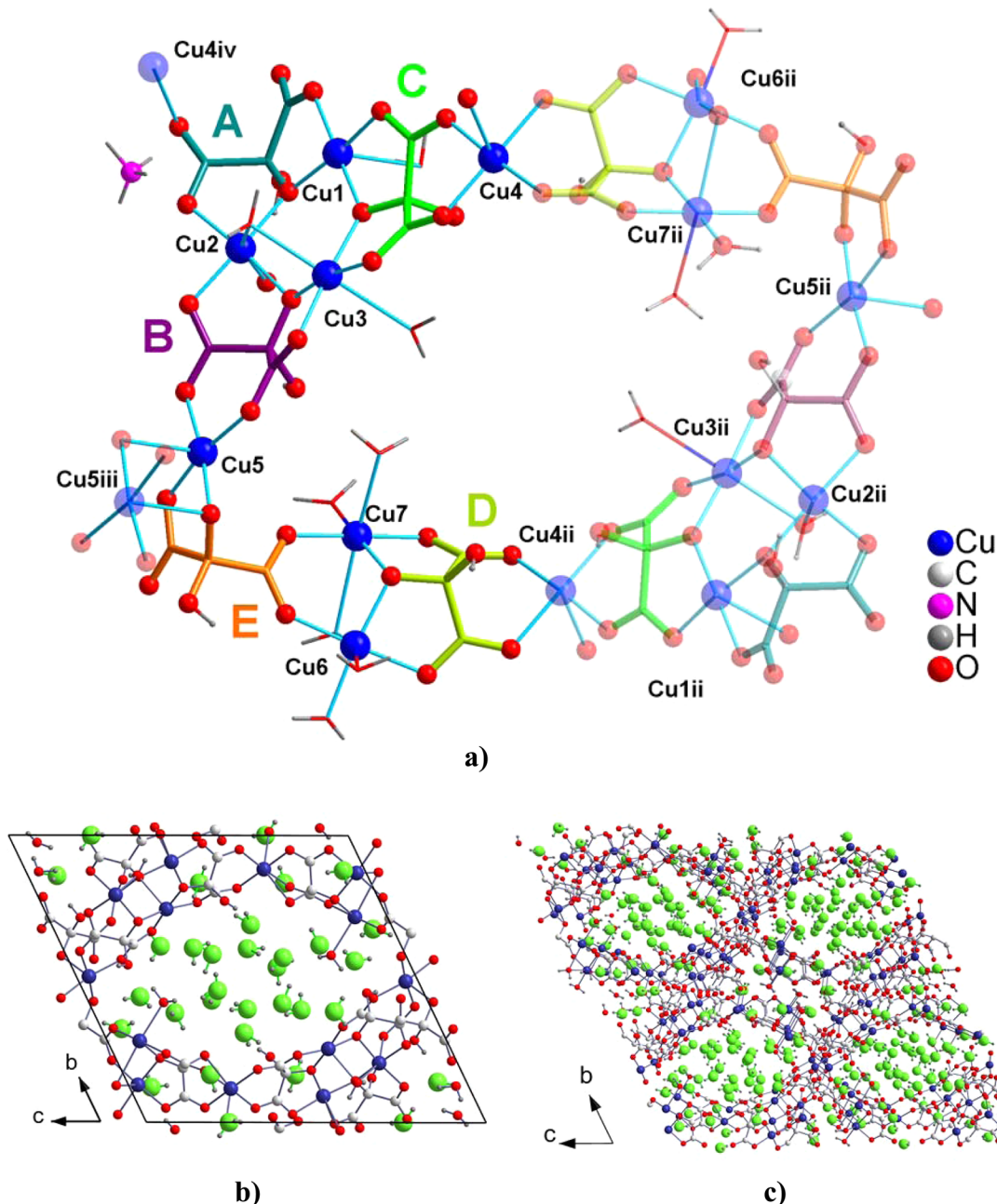
**Synthesis.** Copper(II) mesoxalate aqueous solutions have been observed to form [Cu<sub>3</sub>(Hmesox)<sub>3</sub>]<sup>3-</sup> species<sup>59–61,63</sup> analogous to those formed by tartronic and malic acids (Scheme 1).<sup>64–67</sup> With those solutions as precursor, and following the approach of the reticular synthesis,<sup>6,8</sup> polymeric materials are obtained neutralizing the excess of hydrogen ions and balancing the negative charge of the trinuclear complex with counterions provided by metallic salts. With this

**Scheme 1.** Tartronic, Mesoxalic, and Malic Acids

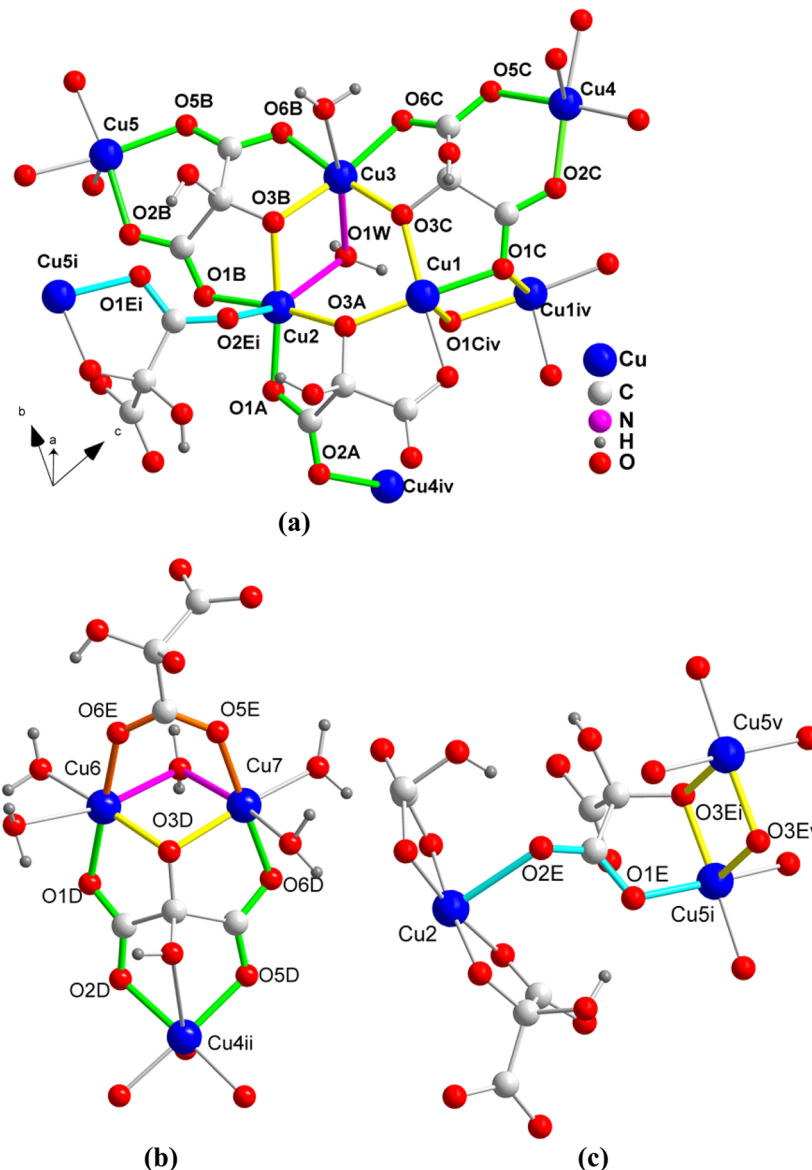
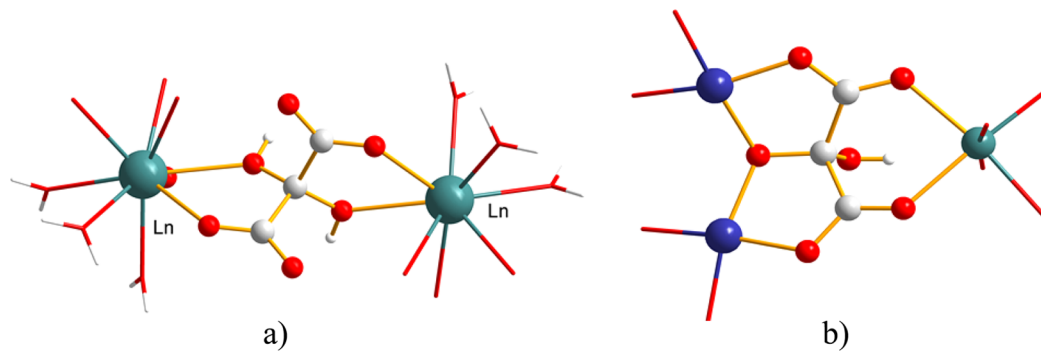
procedure we obtained  $[La(H_2O)_3Cu_3(Hmesox)_3(H_2O)_5] \cdot 8H_2O$  and  $[La(H_2O)_2Cu_3(Hmesox)_3(H_2O)_3] \cdot 7H_2O$  by the addition of  $Li(OH) + La(NO_3)_3$  to the precursor solution.<sup>63</sup>

$K_3[Cu_3(Hmesox)_3]$  was obtained by the addition of KOH.<sup>59</sup> And the addition of M(II) acetate +  $Ph_4PCl$  yielded the compounds  $\{(Ph_4P)_2[M^{II}Cu_3(Hmesox)_3Cl]\}_n$  with M(II) = Mn, Co, and Ni.<sup>59–61</sup>

Following the same strategy, to the solution containing the  $[Cu_3(Hmesox)_3]^{3-}$  species copper(II) nitrate was added to yield the anionic three-dimensional network of **1a** and **1b**. The tetrabutylammonium hydroxide and aqueous ammonia were respectively added to neutralize some of the hydrogen ions of the original solution ( $pH = 2.0$ ). The tetrabutylammonium ions did not fit in the voids of the network, and  $H_3O^+$  ions were included as counterions in  $\{(H_3O)[Cu_7(Hmesox)_5(H_2O)_7] \cdot 9H_2O\}_n$  (**1a**). In the case of  $\{(NH_4)_{0.6}(H_3O)_{0.4}$



**Figure 1.** (a) Two symmetry-related asymmetric units of **1a** (and **1b**). The five crystallographically independent mesoxalate ligands (A–E) are given in different colors. Copper atoms and mesoxalate ligands of a neighboring unit are depicted semitransparent. Symmetry codes: (i)  $1 - x, 1 - y, z$ ; (ii)  $x, y, -1 + z$ ; (iii)  $x, y, 1 + z$ ; (iv)  $-x, 1 - y, -z$ . (b) Projection of the unit cell in the  $bc$  plane. Color scheme: Cu(II), blue; O, red; C, gray; H, dark gray; crystallization water, green molecules. (c) Perspective view of the three-dimensional negatively charged coordination network along the  $a$  axis.

Scheme 2.  $\mu_2$  (a) and  $\mu_3$  (b) Bridging Modes of the Mesoxalate Ligand

**Figure 2.** Bridging modes exhibited by mesoxalate:  $\mu$ -alkoxide (yellow), anti-anti carboxylate (green), syn-syn carboxylate (orange), syn-anti carboxylate (cyan). Bridging mode exhibited by aqua ligands:  $\mu_2$ -OH<sub>2</sub> (pink). (a) Connectivity of Cu1, Cu2, and Cu3 with other copper atoms of neighboring units. (b) Connection of Cu6 and Cu7 with Cu4ii. (c) Connection of Cu5i with Cu2 and Cu5v. Symmetry codes (i) 1 -  $x$ , 1 -  $y$ , - $z$ ; (ii) 1 -  $x$ , 1 -  $y$ , 1 -  $z$ ; (iii) 2 -  $x$ , 1 -  $y$ , - $z$ ; (iv) 1 -  $x$ , - $y$ , 1 -  $z$ ; (v) -1 +  $x$ ,  $y$ ,  $z$ .

[Cu<sub>7</sub>(Hmesox)<sub>5</sub>(H<sub>2</sub>O)<sub>7</sub>]·11H<sub>2</sub>O<sub>n</sub> (**1b**) ammonium cations and together with H<sub>3</sub>O<sup>+</sup> ions neutralize the negative charge of the anionic network.

**Description of the Structures.** The structure of **1a** (and that of **1b**) consists of a low-symmetry copper(II)/mesoxalate(3-) anionic network with H<sub>3</sub>O<sup>+</sup> (and NH<sub>4</sub><sup>+</sup> in

**1b**) cations and water molecules of crystallization in the voids left by the framework (Figure 1). The asymmetric unit contains seven copper(II) ions and five mesoxalate ligands(A–E) (Figure 1a). Cu1, Cu2, and Cu3 with mesoxalates A, B, and C form a trinuclear unit similar to that observed in  $K_3[Cu_3(Hmesox)_3(H_2O)]$ .<sup>59</sup> Cu4 and Cu5 are, respectively, bonded to mesoxalates C and B of the trinuclear unit, and mesoxalate E connects Cu5 with Cu6 and Cu7. The asymmetric unit is completed with mesoxalate D bound to Cu6 and Cu7. A second heptanuclear unit, related to the original by a symmetry center, joins the previous one to yield a circular cluster that contains 14 copper(II) ions and 10 mesoxalate ligands (Figure 1a). The unit cell contains two of these 14-nuclear clusters and crystallization water molecules (Figure 1b). The three-dimensional structure shows water channels parallel to the *a* direction (Figure 1c).

The copper atoms are in square pyramidal (Cu1–Cu4) and Jahn–Teller distorted octahedral (Cu6, Cu7) environments. Mesoxalate carboxylate, mesoxalate alkoxide, and water oxygen atoms constitute their coordination sphere. Main distances and angles in expected ranges are given in Supporting Information, Table S2. The five mesoxalate ligands (A–E) are in the trinegative anionic form (mesoxalic acid =  $H_4\text{mesox}$ ), with one of the alcohol and the two carboxyl groups being deprotonated. Mesoxalates B, C, and E coordinate as pentadentate, A acts as tetridentate, and D acts as hexadentate ligand. Mesoxalates B and C form two five- and one six-membered chelate ring complexing the copper(II) ions. D forms four, A yields two, and E just one five-membered chelate-ring.

**Bridging Modes of the Mesoxalate-Alkoxide and Mesoxalate-Carboxylate Groups.** The main structural feature of **1a** and **1b** is the connectivity displayed by the mesoxalate ligands to link the copper(II) ions within and among the asymmetric units. Up to now, two binding and bridging modes were known for the mesoxalate ligand (Scheme 2): the  $\mu_2$ -H<sub>2</sub>mesoxalate ( $\mu_2$ - $\kappa O,O'':O'',O''')$  was observed in  $[Ln_2(H_2\text{mesox})_3(H_2O)_6]$  and  $\{Na[M(Hmesox)(H_2O)_2]\}_n$ , where Ln are lanthanoid(III) ions and M are Mn(II) and Zn(II);<sup>68–71</sup> and the  $\mu_3$ -Hmesoxalate ( $\mu_3$ - $\kappa O,O'':O'',O''')$  observed in  $\{(Ph_4P)_2[M^{II}Cu_3(Hmesox)_3Cl]\}_n$ ,  $[La(H_2O)_3Cu_3(Hmesox)_3(H_2O)_5] \cdot 8H_2O$ , and  $[La(H_2O)_2Cu_3(Hmesox)_3(H_2O)_3] \cdot 7H_2O$ ,<sup>59–61,69</sup> in which the two carboxylate groups act as bridging groups with the anti–anti 1,3–OCO configuration and one of the hydroxyl groups has been deprotonated and works as bridging  $\mu_2$ -alkoxo.

In **1a** and **1b**, Cu1, Cu2, and Cu3 are bridged by O3A, O3B, and O3C mesoxalate  $\mu_2$ -alkoxide oxygens to yield a triangular cluster similar to that observed in  $\{(Ph_4P)_2[M^{II}Cu_3(Hmesox)_3Cl]\}_n$  (Figure 2a).<sup>59–61</sup> Cu4 is linked to Cu3 and Cu1 through the carboxylate groups of mesoxalate C in the anti–anti bridging mode (Figure 2a). Similarly, Cu5 is connected with Cu2 and Cu3 by two anti–anti carboxylate groups of mesoxalate B (Figure 2a). Cu6 and Cu7 are linked by a syn–syn carboxylate (of mesoxalate E), one  $\mu$ -alkoxide (of mesoxalate D), and one  $\mu$ -aqua bridge (Figure 2b). Although the syn–syn bridging mode is very frequent in carboxylate bridging groups, it is first observed for the mesoxalate ligand in this compound.

Furthermore, the asymmetric unit is part of a three-dimensional metal–ligand network (Figure 1c). Thereby, Cu2 is connected to Cu5i through a syn–anti carboxylate bridge (Figure 2c) and to Cu4iv through a nonplanar anti–anti carboxylate (Figure 2a); Cu5 is connected to Cu5iii through a

double  $\mu$ -alkoxide (Supporting Information, Figure S3); Cu1 and Culiv are connected through double  $\mu$ -carboxylate oxygen (Figure 2a); and Cu6 and Cu7 are connected through anti–anti carboxylate with Cu4ii (Figure 1a). [(i)  $1 - x, 1 - y, -z$ ; (ii)  $1 - x, 1 - y, 1 - z$ ; (iii)  $2 - x, 1 - y, -z$ ; (iv)  $1 - x, -y, 1 - z$ ; (v)  $-1 + x, y, z$ .]

The structure of the compounds is very different from other mesoxalate MOFs, which yielded polymeric structures with much higher symmetry. Lanthanoid(III) mesoxalates with general formula  $\{[Ln_2(\mu-H_2\text{mesox})_3(H_2O)_6]\}_n$  exhibit chiral gray–arsenic-type (6,3)-net.<sup>68,69</sup> The bimetallic  $\{(Ph_4P)_2[M^{II}Cu_3(Hmesox)_3Cl]\}_n$ , with M(II) = Mn, Co, and Ni, yield the chiral cubic three-dimensional (10,3)a network, and the  $\{[La(H_2O)_3Cu_3(Hmesox)_3(H_2O)_5] \cdot 8H_2O\}_n$  and  $\{[La(H_2O)_2Cu_3(Hmesox)_3(H_2O)_3] \cdot 7H_2O\}_n$  yield the two-dimensional hexagonal (6,3) manifolds.<sup>59–61,63</sup> Moreover, in  $\{Na[M(Hmesox)(H_2O)_2]\}_n$  and  $\{Na[Zn(Hmesox)(H_2O)]\}_n$ , the mesoxalate ligand works as trivalent anion resulting in chain structures.<sup>70,71</sup> So, the low-symmetry structure exhibited by **1a** and **1b** is very unusual for mesoxalate-bridged MOFs.

Because of the  $-3$  charge of the mesoxalate linker and the  $+2$  charge of the copper(II) atom there remains a  $-1$  charge for  $[Cu_7(Hmesox)_5(H_2O)_7]^-$  unit, which is balanced by one  $H_3O^+$  cation in **1a** (and a mixture of  $H_3O^+$  and  $NH_4^+$  in **1b**). The cations are located in the voids left by the anionic network together with crystallization water molecules. Some of the water molecules in **1a** are highly disordered with partial occupation, which made their hydrogen atoms impossible to locate. Hence, none of the oxygen atoms of the crystallization water molecules were clearly found to be surrounded by three hydrogen atoms in **1a**, which suggests that the proton is delocalized, and this mobility of the hydrogen atoms is the origin of the proton conductivity.<sup>35–37</sup> In **1b** (at low temperature), the ammonium ion and crystallization water molecules are better observed, and they are found to be organized into pentagonal and octagonal motives along the *a* axis with distances ranging from 2.39 to 3.31 Å (Supporting Information, Figure S4). Some authors explain high proton conductances as a consequence of these organized clusters of water molecules.<sup>42</sup>

**Magnetic Properties.** The temperature dependences of the  $\chi_M$  and  $\chi_M T$  product for compound **1a** are shown in Figure 3a. ( $\chi_M$  is the magnetic susceptibility per seven Cu(II) ions). The value observed for  $\chi_M T$  at room temperature is somewhat lower than that expected for seven noninteracting spin doublets (expected  $\chi_M T = 7x(N\beta^2 g^2/3k)S(S+1) = 2.80 \text{ cm}^3 \text{ mol}^{-1} \text{ K}$  with  $g \approx 2.1$  and  $S = 1/2$ ; observed  $2.16 \text{ cm}^3 \text{ mol}^{-1} \text{ K}$ ), and upon cooling it continuously decreases to reach a minimum at 35 K, then increases, reaching a maximum at  $\sim 10$  K, to decrease again at lower temperatures due to saturation effects (Supporting Information, Figure S7). This behavior is indicative of the occurrence of a long-range ferrimagnetic ordering. The susceptibility versus temperature plot obtained at different fields also reveals the magnetic ordering with an onset temperature just below 20 K and a rounded maximum at 14 K, which corresponds to a weak antiferromagnetic coupling that can be turned off with a field just above 50 Oe (inset of Figure 3a). The magnetic ordering temperature at 17.6 K is established by the out-of-phase magnetic susceptibility measurements shown in Figure 4. The magnetization versus field (H/KOe) isotherm at 2 K is shown in Figure 3b. At fields lower than 40 Oe (Supporting Information, Figure S9) the slope of the plot is very small; above 60 Oe the slope increases and starts to saturate just above 500 Oe, thus exhibiting a sigmoidal shape.

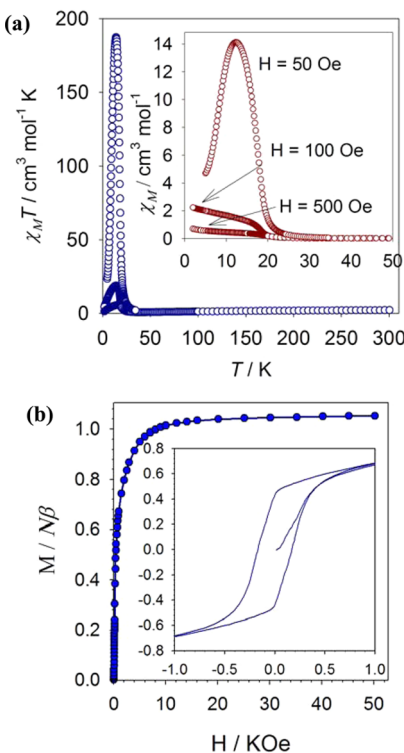


**Figure 3.** (a) Temperature dependence of  $\chi_M$  (inset) and  $\chi_M T$  product for compound **1a** at different applied magnetic fields. (b) Magnetization vs  $H$  plot isotherm at 2 K for compound **1a**. (inset) The hysteresis loop. The solid lines are eye guides.

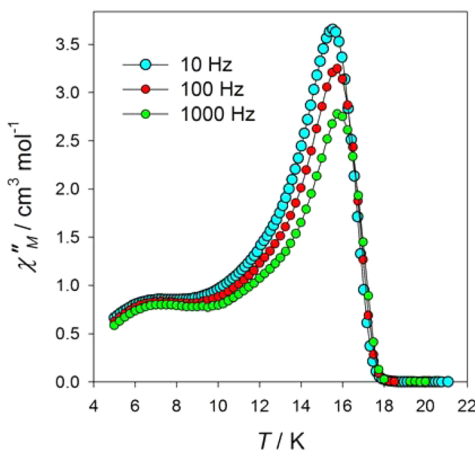


**Figure 4.** Temperature dependence of the out-of-phase component of the ac magnetic susceptibility for compound **1a** at the indicated frequencies.

The value reached at the highest applied field corresponds to one copper(II) ion per formula, and this fact together with the sigmoidal shape of the plot confirms the ferrimagnetic nature of the magnetic ordering. The hysteresis loops shows a coercive field of 350 Oe, in agreement with the isotropic character of the copper(II) ions.

Because of the three-dimensional character of the structure and because of the occurrence of the long-range magnetic ordering, the values of the magnetic coupling constants of the different bridges (coordination water molecules, alkoxide and carboxylate groups of the mesoxalate linker, Figure 2) cannot be calculated, and just a qualitative analysis of the magneto-

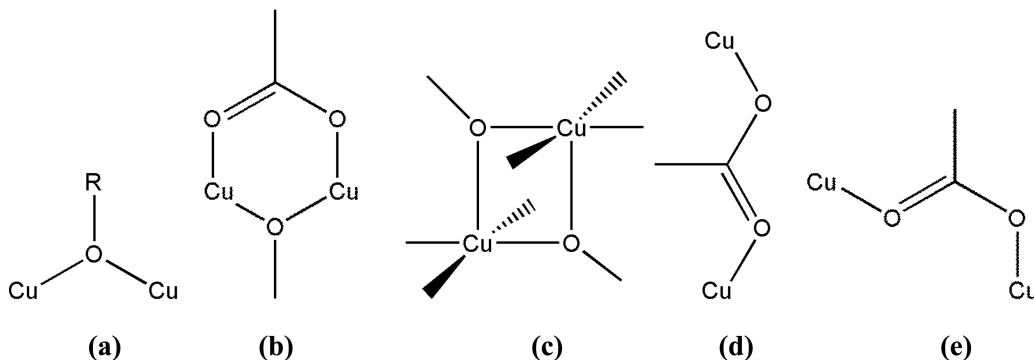
structural correlations can be performed. However, previous magneto-structural studies in these kinds of bridges allow us not only to predict the ferro- or antiferromagnetic nature of the magnetic coupling but also to estimate its intensity, Scheme 3.

The  $\mu_2$ -alkoxide bridge with Cu–O–Cu bridging angles larger than  $98.5^\circ$  is known to couple copper(II) ions antiferromagnetically.<sup>62</sup> However, we have observed that in the copper(II) mesoxalate trinuclear species, because of the large deviation from the planarity, ferromagnetic couplings can be expected between Cu2 and Cu3 with a Cu–O–Cu bridging angle of  $114.8^\circ$  [deviation from the planarity  $48.8(1)^\circ$ ].<sup>60,66,67,72</sup> Additionally, Cu2 and Cu3 are also bridged by an  $\mu_2$ -aqua ligand with a Cu–O–Cu bridging angle of  $83.25^\circ$  so we expect these two ions to be ferromagnetically coupled, but antiferromagnetically coupled Cu1 linked to them via  $\mu_2$ -alkoxide bridges with angles of  $133.48^\circ$  and  $131.50^\circ$  for Cu1–O–Cu3 and Cu1–O–Cu2, respectively.<sup>62</sup> Cu6 and Cu7 are connected via a combined syn–syn  $\mu_2$ -1,3-carboxylate +  $\mu_2$ -alkoxide bridge, which are found to work as ferromagnetic couplers because of the counter-complementarity phenomenon first described by Nishida et al. and McKee et al.<sup>73–77</sup> The rest of copper(II) ions of the asymmetric unit are bridged by anti–anti  $\mu_2$ -1,3-carboxylate bridges (Cu4 with Cu1 and Cu3; Cu5 with Cu2 and Cu3), which couple strongly antiferromagnetically.<sup>78</sup>

The diverse bridging modes exhibited by the ligands lead to ferro- and antiferromagnetic couplings among the copper(II) ions within the asymmetric unit, which results in an incomplete cancellation of their magnetic moments. This particular behavior is known as topological ferrimagnetism,<sup>79–81</sup> and it is very infrequent in copper(II) complexes.<sup>81,82</sup> In addition to these couplings within the asymmetric unit there are multiple couplings with neighboring copper(II) ions, which extend the magnetic coupling along the three-dimensional structure; for instance, Cu2 is linked to Cu4iv and Cu5 is linked to Cu2 via an anti–anti nonplanar equatorial–axial  $\mu_2$ -1,3-carboxylate Cu–O–C–O–Cu exchange pathway, mediating a weak ferromagnetic coupling;<sup>83–85</sup> Cu5 and Cu5iii are linked via two equatorial–apical  $\mu_2$ -alkoxide bridge with a Cu–O axial distance of 2.396 Å, which is said to weakly couple ferromagnetically;<sup>86</sup> and Cu6 and Cu7 are strongly antiferromagnetically coupled to Cu4ii via two anti–anti  $\mu_2$ -1,3-carboxylate bridges.<sup>87,88</sup> This multiple connection leads to the long-range three-dimensional ferrimagnetic ordering. So, this compound is a rare example that illustrates how homospin antiferromagnetic materials can yield long-range magnetic ordering.<sup>89</sup> (i)  $1 - x, 1 - y, -z$ ; (ii)  $1 - x, 1 - y, 1 - z$ ; (iii)  $2 - x, 1 - y, -z$ ; (iv)  $1 - x, -y, 1 - z$ ; (v)  $-1 + x, y, z$ .

The out-of phase ( $\chi''$ ) component of the ac susceptibility is shown in Figure 4. The positive value of  $\chi''$  below 17.6 K is indicative of the long-range magnetic ordering. To this phase transition corresponds the maxima observed at higher temperatures, and it is related to the above-mentioned magnetic coupling extended along the MOF. However, the rounded maxima at lower temperatures and their frequency dependence suggests the occurrence of a spin-glass behavior.<sup>90</sup>

Single-molecule magnets, magnetic nanoparticles, single-chain magnets as well as spin-glass systems show frequency-dependent maxima in ac plots (Supporting Information, Figure S8). The  $F$  ratio has been proposed by Mydosh to distinguish between a spin-glass behavior and the other magnetic systems.<sup>91</sup>  $F$  is defined as  $F = (T_i - T_j)/[T_i(\log(f_i) - \log(f_j))]$  where  $T_i$  and  $T_j$  are the temperatures at which the maxima in  $\chi''$

Scheme 3. Bridging Modes of Alkoxide and Carboxylate Groups of the Mesoxalate Linker Found in **1a** and **1b**<sup>a</sup>

<sup>a</sup>(a)  $\mu_2$ -alkoxide, (b) syn–syn  $\mu_2$ -1,3-carboxylate +  $\mu_2$ -alkoxide, (c) equatorial-apical double  $\mu_2$ -alkoxide, (d) anti–anti  $\mu_2$ -1,3-carboxylate, (e) anti–syn  $\mu_2$ -1,3-carboxylate.

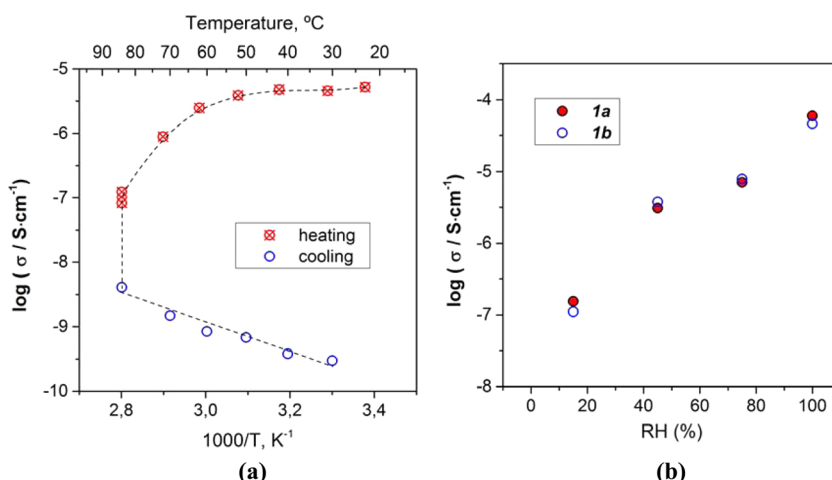


Figure 5. (a) Temperature dependence of the proton conductivity of **1a** in dry air. (b) Dependence of the proton conductivity of **1a** and **1b** on relative humidity (RH) at 23 °C.

occur at frequencies  $f_i$  and  $f_j$ . The  $F$  value for compound **1a** gives a mean value of 0.020(1), which is in agreement with a spin-glass behavior. Thus, the rounded maxima observed in the ac plot at low temperatures would correspond to a spin-glass transition. The spin-glass behavior can be a consequence of the spin frustration that occurs in antiferromagnetically coupled trinuclear clusters.<sup>92</sup> For instance, in **1a**, Cu1, Cu3, and Cu4 are antiferromagnetically connected through one alkoxide and through two anti–anti carboxylate bridges (Figure 1a). The antiferromagnetically coupled trinuclear cluster is a spin-frustrated system, since the spin of the three copper(II) ions cannot be simultaneously antiferromagnetically coupled, and this results in the spin-glass behavior.

**Thermal Stability.** Thermogravimetric (TG) measurements were performed for compounds **1a** and **1b** under dinitrogen atmosphere (Supporting Information, Figure S6a). Both compounds show weakly bound crystal and coordination water molecules (16 and 18 for **1a** and **1b**, respectively), which are lost in a first step from room temperature to 150 °C (measured 19% and 20%, calcd. 20% and 22%, for **1a** and **1b**, respectively), followed by the thermal decomposition of the mesoxalate ligand (150–300 °C) resulting in Cu<sub>2</sub>O (measured 63% and 65%, calcd. 63% and 65%, for **1a** and **1b**, respectively). The thermal stability in air was also measured in a different experiment for compound **1a** to investigate the total amount of water that can be lost at the highest temperature reached in the

conductometric study (Supporting Information, Figure S6b). Thus, temperature was kept constant at 85 °C for 3 h resulting in a weight loss of 20%, which corresponds to 16 water molecules in agreement with the sum of crystallization and coordination water molecules of **1a**. Above 150 °C the decomposition of the ligand occurs, and the weight loss increases up to 65%, which corresponds to the formation of Cu<sub>2</sub>O (calcd. 65% at 250 °C). At higher temperatures, in the air atmosphere, CuO is formed with the consequent regain of weight (measured 62%, calcd. 61%).

**Proton Conduction.** The impedance spectra of **1a** and **1b** obtained under different conditions (Supporting Information, Figure S10) showed one semicircle and a low-frequency tail quite similar to the higher frequency portion of a Warburg element. On the basis of the associated capacitance ( $C_b \approx 5 \times 10^{-12}$  F/cm) the semicircle could be ascribed unequivocally to the bulk conduction, while the low-frequency part of the spectra was indicative of a diffusion-limited electrode response. Partial blocking of ionic charge carriers within the electrode typically results in such low-frequency dispersion pattern, which suggests that the ac conductivity of **1a** and **1b** is actually dominated by protons.<sup>31</sup> As can be seen in Figure 5a the proton conductivity of pristine **1a** ( $\sigma_{H^+} = 5.2 \times 10^{-6}$  S cm<sup>-1</sup>) remains virtually constant on heating to ~40 °C. At higher temperatures, the conductivity gradually decreases and eventually drops dramatically to  $4.1 \times 10^{-9}$  S cm<sup>-1</sup> after a 5 h dwell at 85

°C. Cooling the same sample down, however, brings about further decrease in conductivity, thus implying that elevated temperatures have a profound effect on mobility of protons. Interestingly, such behavior correlates quite well with the TG data (Supporting Information, Figure S6), according to which dehydration of **1a** and **1b** largely takes place below 100 °C. With all these data at hand we argue that proton conduction within the bulk of **1a** seems to be mediated by water molecules and therefore should occur via the Grotthuss mechanism.<sup>41</sup> When heated above 40 °C **1a** progressively loses its crystallization water molecules accommodated inside the hydrophilic channels, which provokes disruption of the proton transport along the hydrogen-bond network and concomitant decrease in conductivity.<sup>42,48</sup>

The above conclusion is further corroborated by the fact that proton conductivity of **1a** and **1b** was found to be almost identical and depend heavily on relative humidity (Figure 5b). Indeed, at 100% relative humidity and 23 °C conductivity of both samples increased by 1 order of magnitude ( $\sigma_{\text{H}^+} \approx 6.5 \times 10^{-5} \text{ S cm}^{-1}$ ) relative to the pristine values and then continuously decreased as the humidity of the surrounding gas was reduced. The highest conductivity reached by **1a** and **1b** is in the range of other magnetic MOFs.<sup>32,33,43,53,54</sup> The almost equivalent behavior of both compounds suggests that both  $\text{H}_3\text{O}^+$  and  $\text{NH}_4^+$  cations play an equal role in proton conduction.

## CONCLUSIONS

The low symmetry and highly connected copper(II)/mesoxalate network of compounds **1a** and **1b** are very different from those of other mesoxalate complexes, which yielded polymeric structures with much higher symmetry, and a new syn-syn carboxylate binding and bridging mode has been found for the mesoxalate ligand. The different kinds of bridging modes between the mesoxalate and the copper(II) ions result in ferro- and antiferromagnetic couplings, which lead to long-range ferrimagnetic ordering with a critical temperature of 17.6 K. Moreover, the compounds exhibit proton conduction with a highest value of  $\sim 6.5 \times 10^{-5} \text{ S cm}^{-1}$ .

## ASSOCIATED CONTENT

### Supporting Information

X-ray crystallographic data acquisition and analysis; crystallographic details; selected bond lengths and angles. Details of the structure; powder diffraction patterns; TG plots; dc magnetic data at 500 Oe; ac magnetic data; low-field magnetization and hysteresis loop; impedance spectra;(CCDC: 1011418–1011419). This material is available free of charge via the Internet at <http://pubs.acs.org>. Crystallographic information in CIF format (CCDC numbers 1011418 and 1011419 for **1a** and **1b**) can be obtained free of charge from the Cambridge Crystallographic Data Centre via [www.ccdc.cam.ac.uk/data\\_reuest/cif](http://www.ccdc.cam.ac.uk/data_reuest/cif).

## AUTHOR INFORMATION

### Corresponding Author

\*E-mail: jsanchiz@ull.es.

### Notes

The authors declare no competing financial interest.

## ACKNOWLEDGMENTS

Financial support from Departamento de Química de la Universidad de La Laguna and Ministerio Español de Ciencia e Innovación through Project No. MAT2010-16981 is acknowledged. B.G.H. acknowledges the grant from Programa FPI of ACIISI from Gobierno de Canarias and Fondo Social Europeo.

## REFERENCES

- (1) Fujita, M.; Kwon, Y. J.; Washizu, S.; Ogura, K. *J. Am. Chem. Soc.* **1994**, *116*, 1151–1152.
- (2) Abrahams, B. F.; Jackson, P. A.; Robson, R. R. *Angew. Chem., Int. Ed.* **1998**, *37*, 2656–2659.
- (3) Janiak, C. *Dalton Trans.* **2003**, 2781–2804.
- (4) Rowsell, J. L. C.; Yaghi, O. M. *Microporous Mesoporous Mater.* **2004**, *73*, 3–14.
- (5) Furukawa, H.; Cordova, K. E.; O'Keeffe, M.; Yaghi, O. M. *Science* **2013**, *341*, 1230444.
- (6) Yaghi, O. M.; O'Keeffe, M.; Ockwig, N. W.; Chae, H. K.; Eddaoudi, M.; Kim, J. *Nature* **2003**, *423*, 705–714.
- (7) Férey, G. *Chem. Soc. Rev.* **2008**, *37*, 191–214.
- (8) Tranchemontagne, D. J.; Mendoza-Cortes, J. L.; O'Keeffe, M.; Yaghi, O. M. *Chem. Soc. Rev.* **2009**, *38*, 1257–1283.
- (9) Murray, L. J.; Dinca, M.; Long, J. R. *Chem. Soc. Rev.* **2009**, *38*, 1294–1314.
- (10) Ma, L.; Abney, C.; Lin, W. *Chem. Soc. Rev.* **2009**, *38*, 1248–1256.
- (11) Ma, S. Q.; Zhou, H. C. *Chem. Commun.* **2010**, *46*, 44–53.
- (12) Sumida, K.; Rogow, D. L.; Mason, J. A.; McDonald, T. M.; Bloch, E. D.; Herm, Z. R.; Bae, T.-H.; Long, J. R. *Chem. Rev.* **2011**, *112*, 724–781.
- (13) Cui, Y.; Yue, Y.; Qian, G.; Chen, B. *Chem. Rev.* **2011**, *112*, 1126–1162.
- (14) Wang, C.; Zhang, T.; Lin, W. *Chem. Rev.* **2011**, *112*, 1084–1104.
- (15) Yoon, M.; Srirambalaji, R.; Kim, K. *Chem. Rev.* **2012**, *112*, 1196–1231.
- (16) Janiak, C.; Vieth, J. K. *New J. Chem.* **2010**, *34*, 2366–2388.
- (17) Wu, L.; Xue, M.; Qiu, S.-L.; Chaplais, G.; Simon-Masseron, A.; Patarin, J. *Microporous Mesoporous Mater.* **2012**, *157*, 75–81.
- (18) Li, J.-R.; Kuppler, R. J.; Zhou, H.-C. *Chem. Soc. Rev.* **2009**, *38*, 1477–1504.
- (19) Suh, M. P.; Park, H. J.; Prasad, T. K.; Lim, D.-W. *Chem. Rev.* **2011**, *112*, 782–835.
- (20) Bétard, A.; Fischer, R. A. *Chem. Rev.* **2011**, *112*, 1055–1083.
- (21) Tamaki, H.; Zhong, Z. J.; Matsumoto, N.; Kida, S.; Koikawa, M.; Achiwa, N.; Hashimoto, Y.; Okawa, H. *J. Am. Chem. Soc.* **1992**, *114*, 6974–6979.
- (22) Decurtins, S.; Schmalle, H. W.; Oswald, H. R.; Linden, A.; Enslin, J.; Gülich, P.; Hauser, A. *Inorg. Chim. Acta* **1994**, *216*, 65–73.
- (23) Mathoniere, C.; Nuttall, C. J.; Carling, S. G.; Day, P. *Inorg. Chem.* **1996**, *35*, 1201–1206.
- (24) Clemente-León, M.; Coronado, E.; Martí-Gastaldo, C.; Romero, F. M. *Chem. Soc. Rev.* **2011**, *40*, 473–497.
- (25) Stumpf, H. O.; Ouahab, L.; Pei, Y.; Grandjean, D.; Kahn, O. *Science* **1993**, *261*, 447–449.
- (26) Lloret, F.; Julve, M.; Ruiz, R.; Journaux, Y.; Nakatani, K.; Kahn, O.; Sletten, J. *Inorg. Chem.* **1993**, *32*, 27–31.
- (27) Ferlay, S.; Mallah, T.; Ouahès, R.; Veillet, P.; Verdaguier, M. *Nature* **1995**, *378*, 701–703.
- (28) Holmes, S. M.; Girolami, G. S. *J. Am. Chem. Soc.* **1999**, *121*, 5593–5594.
- (29) Hatlevik, Ø.; Buschmann, W. E.; Zhang, J.; Manson, J. L.; Miller, J. S. *Adv. Mater.* **1999**, *11*, 914–918.
- (30) Ohba, M.; Okawa, H. *Coord. Chem. Rev.* **2000**, *198*, 313–328.
- (31) Bureekaew, S.; Horike, S.; Higuchi, M.; Mizuno, M.; Kawamura, T.; Tanaka, D.; Yanai, N.; Kitagawa, S. *Nat. Mater.* **2009**, *8*, 831–836.

- (32) Sadakiyo, M.; Yamada, T.; Kitagawa, H. *J. Am. Chem. Soc.* **2009**, *131*, 9906–9907.
- (33) Sadakiyo, M.; Okawa, H.; Shigematsu, A.; Ohba, M.; Yamada, T.; Kitagawa, H. *J. Am. Chem. Soc.* **2012**, *134*, 5472–5475.
- (34) Taylor, J. M.; Mah, R. K.; Moudrakovski, I. L.; Ratcliffe, C. I.; Vaidhyanathan, R.; Shimizu, G. K. *J. Am. Chem. Soc.* **2010**, *132*, 14055–14057.
- (35) Horike, S.; Umeyama, D.; Inukai, M.; Itakura, T.; Kitagawa, S. *J. Am. Chem. Soc.* **2012**, *134*, 7612–7615.
- (36) Horike, S.; Umeyama, D.; Kitagawa, S. *Acc. Chem. Res.* **2013**, *46*, 2376–2384.
- (37) Kundu, T.; Sahoo, S. C.; Banerjee, R. *Chem. Commun.* **2012**, *48*, 4998–5000.
- (38) Umeyama, D.; Horike, S.; Inukai, M.; Itakura, T.; Kitagawa, S. *J. Am. Chem. Soc.* **2012**, *134*, 12780–12785.
- (39) Wu, B.; Lin, X.; Ge, L.; Wu, L.; Xu, T. *Chem. Commun.* **2013**, *49*, 143–145.
- (40) Xu, G.; Otsubo, K.; Yamada, T.; Sakaida, S.; Kitagawa, H. *J. Am. Chem. Soc.* **2013**, *135*, 7438–7441.
- (41) Yoon, M.; Suh, K.; Natarajan, S.; Kim, K. *Angew. Chem., Int. Ed.* **2013**, *52*, 2688–2700.
- (42) Bazaga-Garcia, M.; Colodrero, R. M.; Papadaki, M.; Garczarek, P.; Zon, J.; Olivera-Pastor, P.; Losilla, E. R.; Leon-Reina, L.; Aranda, M. A.; Choquesillo-Lazarte, D.; Demadis, K. D.; Cabeza, A. *J. Am. Chem. Soc.* **2014**, *136*, 5731–5739.
- (43) Pardo, E.; Train, C.; Gontard, G.; Boubekeur, K.; Fabelo, O.; Liu, H.; Dkhil, B.; Lloret, F.; Nakagawa, K.; Tokoro, H.; Ohkoshi, S.; Verdaguera, M. *J. Am. Chem. Soc.* **2011**, *133*, 15328–15331.
- (44) Shimizu, G. K.; Taylor, J. M.; Kim, S. *Science* **2013**, *341*, 354–355.
- (45) Ramaswamy, P.; Matsuda, R.; Kosaka, W.; Akiyama, G.; Jeon, H. J.; Kitagawa, S. *Chem. Commun.* **2014**, *50*, 1144–1146.
- (46) Ramaswamy, P.; Wong, N. E.; Shimizu, G. K. H. *Chem. Soc. Rev.* **2014**, *43*, 5913–5932.
- (47) Nagarkar, S. S.; Unni, S. M.; Sharma, A.; Kurungot, S.; Ghosh, S. K. *Angew. Chem., Int. Ed.* **2014**, *53*, 2638–2642.
- (48) Phang, W. J.; Lee, W. R.; Yoo, K.; Ryu, D. W.; Kim, B. S.; Hong, C. S. *Angew. Chem., Int. Ed.* **2014**, *53*, 8383–8387.
- (49) Norby, T. J. *Chem. Eng. Jpn.* **2007**, *40*, 1166–1171.
- (50) Sanvito, S. *Chem. Soc. Rev.* **2011**, *40*, 3336–3355.
- (51) Tokoro, H.; Ohkoshi, S.-i. *Dalton Trans.* **2011**, *40*, 6825–6833.
- (52) Ohkoshi, S.-i.; Nakagawa, K.; Tomono, K.; Imoto, K.; Tsunobuchi, Y.; Tokoro, H. *J. Am. Chem. Soc.* **2010**, *132*, 6620–6621.
- (53) Okawa, H.; Sadakiyo, M.; Yamada, T.; Maesato, M.; Ohba, M.; Kitagawa, H. *J. Am. Chem. Soc.* **2013**, *135*, 2256–2262.
- (54) Okawa, H.; Shigematsu, A.; Sadakiyo, M.; Miyagawa, T.; Yoneda, K.; Ohba, M.; Kitagawa, H. *J. Am. Chem. Soc.* **2009**, *131*, 13516–13522.
- (55) Sanchez, C.; Julián, B.; Belleville, P.; Popall, M. *J. Mater. Chem.* **2005**, *15*, 3559–3592.
- (56) Hurd, J. A.; Vaidhyanathan, R.; Thangadurai, V.; Ratcliffe, C. I.; Moudrakovski, I. L.; Shimizu, G. K. H. *Nat. Chem.* **2009**, *1*, 705–710.
- (57) Colodrero, R. M. P.; Olivera-Pastor, P.; Losilla, E. R.; Hernández-Alonso, D.; Aranda, M. A. G.; Leon-Reina, L.; Rius, J.; Demadis, K. D.; Moreau, B.; Villemin, D.; Palomino, M.; Rey, F.; Cabeza, A. *Inorg. Chem.* **2012**, *51*, 7689–7698.
- (58) Colodrero, R. M. P.; Papathanasiou, K. E.; Stavrianoudaki, N.; Olivera-Pastor, P.; Losilla, E. R.; Aranda, M. A. G.; León-Reina, L.; Sanz, J.; Sobrados, I.; Choquesillo-Lazarte, D.; García-Ruiz, J. M.; Atienzar, P.; Rey, F.; Demadis, K. D.; Cabeza, A. *Chem. Mater.* **2012**, *24*, 3780–3792.
- (59) Sanchiz, J.; Pasán, J.; Fabelo, O.; Lloret, F.; Julve, M.; Ruiz-Pérez, C. *Inorg. Chem.* **2010**, *49*, 7880–7889.
- (60) Gil-Hernández, B.; Gili, P.; Vieth, J. K.; Janiak, C.; Sanchiz, J. *Inorg. Chem.* **2010**, *49*, 7478–7490.
- (61) Gil-Hernández, B.; Gili, P.; Sanchiz, J. *Inorg. Chim. Acta* **2011**, *371*, 47–52.
- (62) Kahn, O. *Molecular Magnetism*; VCH: New York, 1993.
- (63) Gil-Hernández, B.; Gili, P.; Pasán, J.; Sanchiz, J.; Ruiz-Pérez, C. *CrystEngComm* **2012**, *14*, 4289–4297.
- (64) Popovich, G. A.; Ablov, A. V. *Zh. Neorg. Khim.* **1967**, *12*, 1552–1556.
- (65) Ablov, A. V.; Popovich, G. A.; Dimitrova, G. I.; Kiosse, G. A.; Burshtein, I. F.; Malinovsky, T. I.; Tscherdvin, B. M. *Dokl. Akad. Nauk SSSR* **1976**, *229*, 611–613.
- (66) Gautier-Luneau, I.; Phanon, D.; Duboc, C.; Luneau, D.; Pierre, J.-L. *Dalton Trans.* **2005**, 3795–3799.
- (67) Pascu, G.; Deville, C.; Clifford, S. E.; Guenée, L.; Besnard, C.; Kramer, K. W.; Liu, S.-X.; Decurtins, S.; Tuna, F.; McInnes, E. J. L.; Winpenny, R. E. P.; Williams, A. F. *Dalton Trans.* **2014**, *43*, 656–662.
- (68) Gil-Hernández, B.; Höppe, H. A.; Vieth, J. K.; Sanchiz, J.; Janiak, C. *Chem. Commun.* **2010**, *46*, 8270–8272.
- (69) Gil-Hernández, B.; MacLaren, J. K.; Höppe, H. A.; Pasán, J.; Sanchiz, J.; Janiak, C. *CrystEngComm* **2012**, *14*, 2635–2644.
- (70) Shi, J.-M.; Zhu, S.-C.; Liu, W.-D. *Trans. Met. Chem.* **2004**, *29*, 358–360.
- (71) Shi, J.-M.; Zhu, S.-C.; Wu, C.-J. *Jiegou Huaxue* **2004**, *23*, 1027–1029.
- (72) Ruiz, E.; Alemany, P.; Alvarez, S.; Cano, J. *J. Am. Chem. Soc.* **1997**, *119*, 1297–1303.
- (73) Christou, G.; Perlepes, S. P.; Libby, E.; Folting, K.; Huffman, J. C.; Webb, R. J.; Hendrickson, D. N. *Inorg. Chem.* **1990**, *29*, 3657–3666.
- (74) Fabelo, O.; Cañadas-Delgado, L.; Pasán, J.; Delgado, F. S.; Lloret, F.; Cano, J.; Julve, M.; Ruiz-Pérez, C. *Inorg. Chem.* **2009**, *48*, 11342–11351.
- (75) Gutierrez, L.; Alzuet, G.; Real, J. A.; Cano, J.; Borrás, J.; Castineiras, A. *Inorg. Chem.* **2000**, *39*, 3608–3614.
- (76) Nishida, Y.; Kida, J. *J. Chem. Soc., Dalton Trans.* **1986**, 2633–2640.
- (77) McKee, V.; Zvagulis, M.; Reed, C. A. *Inorg. Chem.* **1985**, *24*, 2914–2919.
- (78) Julve, M.; Verdaguera, M.; Gleizes, A.; Philoche-Levisalles, M.; Kahn, O. *Inorg. Chem.* **1984**, *23*, 3808–3818.
- (79) Gao, E. Q.; Yue, Y. F.; Bai, S. Q.; He, Z.; Yan, C. H. *J. Am. Chem. Soc.* **2004**, *126*, 1419–1429.
- (80) Zou, J. Y.; Shi, W.; Xu, N.; Li, L. L.; Tang, J. K.; Gao, H. L.; Cui, J. Z.; Cheng, P. *Chem. Commun.* **2013**, *49*, 8226–8228.
- (81) Escuer, A.; Mautner, F. A.; Sodin, B.; Goher, M. A.; Vicente, R. *Dalton Trans.* **2010**, *39*, 4482–4484.
- (82) Chen, Z.; Liu, L.; Wang, Y.; Zou, H.; Zhang, Z.; Liang, F. *Dalton Trans.* **2014**, *43*, 8154–8157.
- (83) Delgado, F. S.; Sanchiz, J.; Ruiz-Pérez, C.; Lloret, F.; Julve, M. *Inorg. Chem.* **2003**, *42*, 5938–5948.
- (84) Colacio, E.; Ghazi, M.; Kivekäs, R.; Moreno, J. M. *Inorg. Chem.* **2000**, *39*, 2882–2890.
- (85) Pasan, J.; Delgado, F. S.; Rodriguez-Martin, Y.; Hernandez-Molina, M.; Ruiz-Perez, C.; Sanchiz, J.; Lloret, F.; Julve, M. *Polyhedron* **2003**, *22*, 2143–2153.
- (86) Baldoma, R.; Monfort, M.; Ribas, J.; Solans, X.; Maestro, M. A. *Inorg. Chem.* **2006**, *45*, 8144–8155.
- (87) Ruiz-Perez, C.; Sanchiz, J.; Molina, M. H.; Lloret, F.; Julve, M. *Inorg. Chem.* **2000**, *39*, 1363–1370.
- (88) Rodriguez-Fortea, A.; Alemany, P.; Alvarez, S.; Ruiz, E. *Chem.—Eur. J.* **2001**, *7*, 627–637.
- (89) Konar, S.; Mukherjee, P. S.; Zangrandi, E.; Lloret, F.; Chaudhuri, N. R. *Angew. Chem., Int. Ed.* **2002**, *41*, 1561–1563.
- (90) Gengler, R. Y.; Toma, L. M.; Pardo, E.; Lloret, F.; Ke, X.; Van Tendeloo, G.; Gournis, D.; Rudolf, P. *Small* **2012**, *8*, 2532–2540.
- (91) Mydosh, J. A. *Spin Glasses: an Experimental Introduction*; Taylor & Francis: London, U.K., 1993.
- (92) Ferrer, S.; Lloret, F.; Pardo, E.; Clemente-Juan, J. M.; Liu-González, M.; García-Granda, S. *Inorg. Chem.* **2012**, *51*, 985–1001.